

LAViTéR: Learning Aligned Visual and Textual Representations Assisted by Image and Caption Generation

Mohammad Abuzar Shaikh* Zhanghexuan Ji* Dana Moukheiber Yan Shen
Sargur Srihari Mingchen Gao

Department of Computer Science and Engineering, University at Buffalo,
The State University of New York, Buffalo, NY, USA

{mshaikh2, zhanghex, danamouk, yshen22, srihari, mgao8}@buffalo.edu

Abstract

Pre-training visual and textual representations from large-scale image-text pairs is becoming a standard approach for many downstream vision-language tasks. The transformer-based models learn inter- and intra-modal attention through a list of self-supervised learning tasks. This paper proposes LAViTéR, a novel architecture for visual and textual representation learning. The main module, Visual Textual Alignment (VTA) will be assisted by two auxiliary tasks, GAN-based image synthesis and Image Captioning. We also propose a new evaluation metric measuring the similarity between the learnt visual and textual embedding. The experimental results on two public datasets, CUB and MS-COCO, demonstrate superior visual and textual representation alignment in the joint feature embedding space. Our code is available at <https://github.com/mshaikh2/LAViTéR>

1. Introduction

Learning cross-modal visual and textual representation is essential for bridging the semantic gap between images and languages. It is the cornerstone for a wide range of vision-language (V+L) tasks, such as image-text cross-modal retrieval, visual question answering (VQA) [2], image captioning [2], and so on.

Inspired by the success of BERT [9] and XLNet [48] using self-supervised learning on natural language processing, there has been a surging research interest in vision-language pre-training on image-text pairs. The learned task-agnostic representation is shown to be effective for many image-language applications after fine-tuning on specific down-

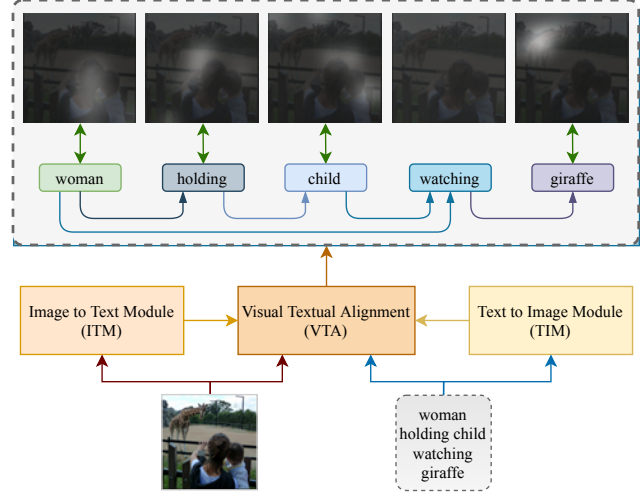


Figure 1: An overview of the end-to-end LAViTéR network. VTA module is assisted by ITM and TIM modules, which in-turn learns to better align the corresponding visual and textual counterparts. The bidirectional arrows indicate the alignment between words and their respective objects in the given image. The intra-word arrows indicate the relationships between the input words that the network learns.

stream tasks. Self-supervised learning is designed to explore the organization of the data as its own source of supervision. This promising approach releases the burden of annotating data with ground truth labels, provides an opportunity to explore a large amount of unlabeled data such as image-text pairs, video-text pairs in free form format from online platforms. This approach has been applied to radiology images combined with their associated reports [24, 5] to leverage the abundance of unlabeled medical data. This

*equal contributions.

data can retrospectively be collected from clinical routine, and has a lot of potential for self-supervised learning.

The representation alignment can be roughly classified into two categories, one-to-one matching and many-to-many matching. One-to-one matching focuses on the global representation from images and sentences, and then associates them by exploiting visual-semantic embedding [43]. Many-to-many matching methods incorporate relationship between regions of a image and words of a sentence to capture fine-grained cross-modal matching [19].

Analogous to the pre-training task in BERT, some pre-training tasks for image-text pairs include the Masked Language Modeling conditioned on image regions and Masked Region Modeling conditioned on input text. Those approaches randomly mask some words or regions from the input and use a Transformer model to recover the words or regions. Many of the fine-grained region-word matching rely on the modern object detectors [6, 23, 44], usually Faster R-CNN [33], to detect salient regions and match them to words. However, the state-of-the-art object detection, which needs to leverage large amount of annotated bounding boxes for supervised learning, is not always available for domain-specific datasets.

Motivated by the above discussion, we propose a model for **L**earning **A**ligned **V**isual and **T**extual **R**epresentation (**LAViT****R**). As shown in Figure 1, the main goal of LAViT R is to learn the joint multi-modal embedding using visual textual alignment (VTA) module, which is assisted by two other self-supervised modules, the text-to-image module (TIM) and image-to-text module (ITM). The method was inspired by CycleGAN [52] and its extension MirrorGAN [31] on image synthesis. In our model, the given images and text are encoded to generate corresponding text and images, respectively. The generated text and images are trained to be mapped back to the original images and text in a cycle. Not only the features learned from real image-text pairs are aligned in the VTA module, the features learned from real-image-fake-text pairs and the fake-image-real-text pairs will also assist the representation learning and alignment. These generated images and texts can provide much more samples outside the training set and make our model more diverse and robust to changes in real data. The proposed method uses high-level features without any explicit supervision, avoiding explicit object detection. Our approach is suitable for the situations where the state-of-the-art object detection model is not feasible, and where bounding box annotations are not available for training.

Our contributions are summarized as follows: 1) We introduce LAViT R for the image-text representation for V+L tasks. 2) We introduce two auxiliary pre-training tasks, GAN-based image synthesis and image captioning, to assist the representation learning. 3) We propose to use a new metric to quantitatively evaluate the similarity between the

image and text representation in the embedded space.

2. Related Work

In this section, we discuss related work about multi-model representation learning and alignment. We also briefly review two main tasks in our architecture to pre-train the joint representation, the GAN-based image generation and image captioning.

2.1. Multi Model Representation Learning

VilBERT [26] and LXMERT [37] are the two pioneering works in image-text joint representation learning, utilizing two streams of Transformers to images and text independently. Those image and text representations then fused by a self-attention mechanism in the later stage. After those two pioneered work, single-stream architecture has also been proposed using a single Transformer to jointly learn image-text embedding, such as UNITER [6], VisualBERT [22], Unicoder-VL [21], VL-VERT [35], B2T2 [1]. Typical self-supervised learning tasks, such as masked language modeling, masked region modeling, image-text matching, and word-region alignment are applied to pre-train the models. More recently, VILLA has been proposed using adversarial training as a general framework can be applied to any V+L models [11].

There are quite a lot of work trying to explicitly enforce the word and region alignment, such as VisualBERT [22], UNITER [6], Oscar [23], MMAC [44]. For example, UNITER [6] uses the Optimal Transport [30] to explicitly calculate the minimum cost of transporting between the image embedding to word embedding.

2.2. Text to Image Generation

Image synthesis from text is a fundamental task in multi-modal learning across vision and language. Most proposed works in image generation are based on conditional Generative Adversarial Networks (GAN). A common approach utilizes a text encoder, mostly RNN-based text encoder before the popularity of Transformer, to encode the text description to guide the image generator [32, 50]. The attention mechanism is widely used to guide the generator to focus on certain words when generating specific regions [47]. The attention mechanism is used to capture the similarity between the generated images and the sentences in both the global level and fine-grained word/region level. MirrorGAN [31], tries to learn better text-to-image generation by re-describing the generated images.

2.3. Image Captioning

Image Captioning is the reverse process of text-to-image generation. It typically consists of a CNN encoder and an RNN decoder to transfer the information from images to

the generated text description [41]. Attention mechanism has been shown very effective focusing on salient objects while generating the corresponding words [46]. Following the success of Faster-RCNN [33] in object detection, bottom-up features provide informative regions in the image, which are used for region level attention [2, 17] and visual scene graph modeling [49]. Recently, transformer architecture [39] is also used for image captioning, which further boosts the captioning performance with its implicit self-attention mechanism [14, 15, 51].

3. Learning Aligned Visual and Textual Representations

As shown in Figure 2, our proposed Learning Aligned Visual and Textual Representations (LAViT-R) model consists of three modules: the visual text alignment (VTA) module, which contains image encoder F_I and text encoder F_T ; the text-to-image (TIM) module, which is the image generator G ; and image-to-text (ITM) module with the text generator C . VTA learns visual-text representations via matching real image-text pairs as our main task. In addition, we introduce two novel assisting tasks, illustrated in blue and green dashed boxes, for a better representation learning: fake-image-real-text matching with fake images generated from TIM; and real-image-fake-text matching where fake texts are converted from ITM using VTA image representations. Meanwhile, both TIM and ITM are also trained on their own losses. We will introduce each of them in the following part of this section.

3.1. VTA: Visual Text Alignment

Given an image-text tuple $\langle I_i, T_i \rangle$, we want to learn the alignment between the words in T_i and the parts of image I_i . For this, we first extract the global features v and local features r using an InceptionV3 [36] based image encoder, where $r \in \mathbb{R}^{D \times M}$ is flattened from the intermediate feature map of ‘mixed_6e’ layer and $v \in \mathbb{R}^D$ from the last average pooling layer. Both of them are projected to the representation feature space with a projection layer. This is denoted as a function F_I in Figure 2, such that $r, v = F_I(I)$. Next, we extract sentence and word level features s and w respectively using a Transformer [39] based text encoder. In Figure 2, this text encoder is denoted as a function F_T , such that, $w, s = F_T(T)$, where $w \in \mathbb{R}^{D \times N}$ and $s \in \mathbb{R}^D$.

We define the F_T as follows: Given text $T \in \mathbb{R}^N$, we use word-based token to embed it as $e \in \mathbb{R}^{D \times N}$, which is summed with positional encoding as the input of F_T . In transformer encoder layer, e is first transformed into queries $Q = W_Q^T e$, keys $K = W_K^T e$ and values $V = W_V^T e$ within each attention head, where $W_Q, W_K, Q_V \in \mathbb{R}^{D \times D_k}$ in our setting. Then “scaled dot-product self-attention” is applied

to e as follows:

$$\text{Attention}(Q, K, V) = f_s\left(\frac{QK^T}{\sqrt{D_k}}\right)V \quad (1)$$

where f_s is the softmax function.

Multi-head attention is applied to the self-attention sub-layer and the outputs from h heads are concatenated:

$$\begin{aligned} \text{head}_i &= \text{Attention}(W_{Q_i}^T e, W_{K_i}^T e, W_{V_i}^T e) \\ \text{Multihead}(e) &= W_O \text{Concat}(\text{head}_1, \dots, \text{head}_h) \end{aligned} \quad (2)$$

where $W_O \in \mathbb{R}^{D \times hD_k}$.

The output from the multi-head attention is then sent to a feed-forward network. The residual mechanism [13] and layer normalization are applied to multi-head attention and FFN outputs:

$$\begin{aligned} \tilde{e} &= \text{LayerNorm}(e + \text{Multihead}(e)) \\ w &= \text{LayerNorm}(\tilde{e} + \text{FFN}(\tilde{e})) \end{aligned} \quad (3)$$

and $s = \bar{w}$ is used as the sentence representation feature.

Similar to [47] we align the word to image regions by implementing a word-level attention mechanism. First, the word-region attention score α is obtained by multiplying the query, w with context, r , and then normalizing the product using softmax. Next α is multiplied with the context r to obtain the contextual vector c .

$$\begin{aligned} m &= w^T \cdot r \\ \alpha &= f_{s_M}(\gamma_1 f_{s_N}(m)) \\ c &= r \odot \alpha \end{aligned} \quad (4)$$

Where $m \in \mathbb{R}^{N \times M}$ is the match vector; f_{s_N} is the soft-max operation along N words in text T_i ; f_{s_M} is the soft-max operation along M sub-regions of image I_i ; γ_1 is a hyper-parameter to tune the required amount of visual attention for a word and \odot is a matrix multiplication operation. Next, we calculate the element wise cosine similarity between c and w as $\cos = (c^T w) / (\|c\| \|w\|)$ and compute the image to text matching score S by following the work done in [3, 45]:

$$S(I_i, T_i) = \log\left(\sum_{i=1}^{N-1} \exp(\gamma_2 \cos)\right)^{\frac{1}{\gamma_2}} \quad (5)$$

where γ_2 is the importance magnification factor of the most relevant word and image sub-region in the given pair $\langle I_i, T_i \rangle$.

Finally, inspired by [10, 18], we calculate the posterior probability P of image I_i matching with text T_i in a batch of B paired samples:

$$\begin{aligned} P(I_i, T_i) &= f_{s_B}(\gamma_3 S(I_i, T_i)) \\ L_{m_w}^{IT} &= -\log(P(I_i, T_i)) \end{aligned} \quad (6)$$

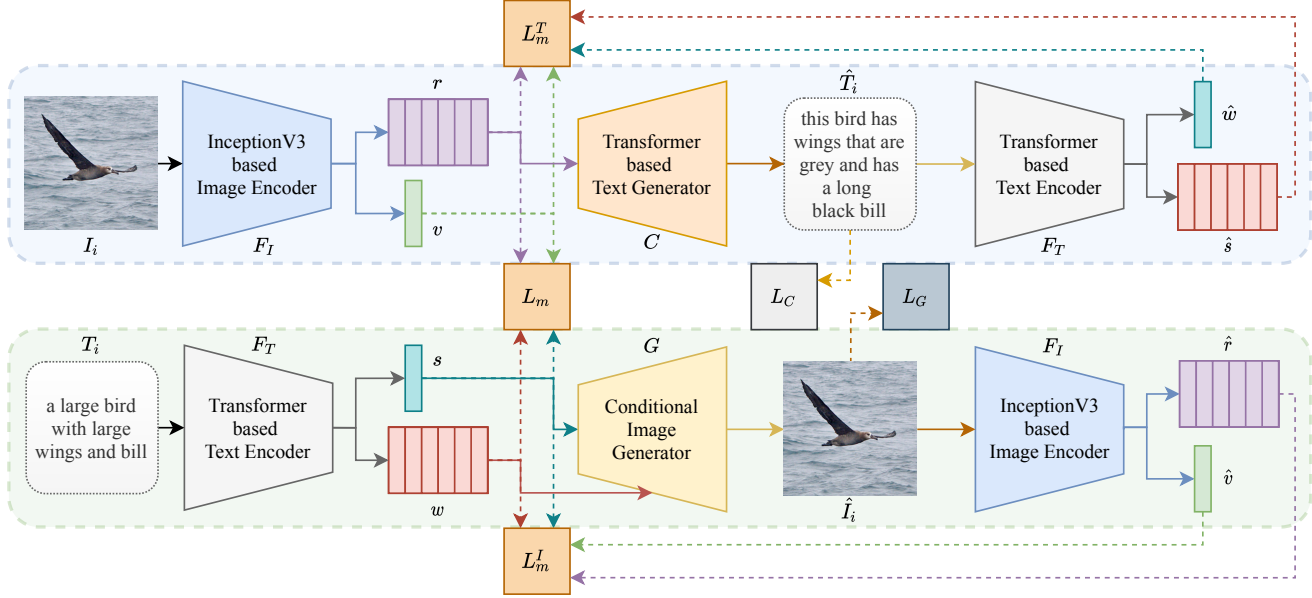


Figure 2: The architecture of the proposed LAViTéR. The pipelines with dotted outlines are the two assisting tasks, namely image to text and text to image conversion. Feature vectors of real image regions are indicated by r while v denotes the global image feature vector. Real text sentence level feature vector is indicated by s while w denotes the word level feature vectors. Similarly all $\hat{w}, \hat{s}, \hat{r}, \hat{v}$ indicates the features extracted from generated samples. L stands for various losses. Dotted arrows indicate the vectors that contribute the loss. Solid arrows indicate the vectors are input to the subsequent network.

where f_{s_B} is the soft-max of matching score S over B paired samples and γ_3 is a hyper-parameter and $L_{m_w}^{IT}$ is the loss when features of image sub-regions r are matched to features of words w in text. Here, the text and image samples at different index are considered as negative pairs and the samples at same index are considered positive pairs. To maintain the symmetry, we also calculate $L_{m_w}^{TI}$ where the image and text variables are switched:

$$P(T_i, L_i) = f_{s_B}(\gamma_3 S(T_i, L_i)) \quad (7)$$

$$L_{m_w}^{TI} = -\log(P(T_i, L_i))$$

Furthermore, we calculate the sentence level matching loss $L_{m_s}^{IT}$ by computing cosine similarity between global vectors v and s as $\cos = (v^T s) / (\|v\| \|s\|)$ and substituting the value of \cos in Equation 5, 6 and 8. Similar to before we can calculate $L_{m_s}^{TI}$ by switching s and v . Thus we compute the total matching loss by adding all the losses.

$$L_m = L_{m_s}^{TI} + L_{m_s}^{IT} + L_{m_w}^{TI} + L_{m_w}^{IT} \quad (8)$$

During the first phase of training the objective is to reduce L_m for pairs of real image I and corresponding text T . For this training we preset $\gamma_1, \gamma_2, \gamma_3$ as per the settings defined in [47] and the batch size $B = 8$.

3.2. TIM: Text to Image Module

To learn the parameters for transforming the textual domain to visual counterpart we use Conditional Generative Adversarial Networks [12, 28] with the sentence vector s as the conditional input. Inspired by the AttnGAN [47], we employ a cascade of GANs. Formally, our TIM task has k discriminators with coupled generators $G \in \{G_1 \dots G_k\}$ that generate images $\hat{I} \in \{\hat{I}_{i1} \dots \hat{I}_{ik}\}$ of different scales, where the suffix i indicate the i^{th} datapoint. We utilize only the output of the k^{th} generator for calculating the assisted losses explained in Equation 15.

We first transform a real text sample T_i using the transformer [39] based text encoder F_T to output a sentence vector s and word vector $w \in \mathbb{R}^{D \times N}$. We denote the entire image generation system, including generators and discriminators as a function G as displayed in Figure 2. A 1-D uniformly sampled random noise vector z along with w as condition, are merged and fed as input to G which outputs an RGB image \hat{I}_i corresponding to T_i .

The image generative loss L_G is thus calculated in an adversarial setup and is defined as follows:

$$L_G = -\frac{1}{2} \mathbb{E}_{\hat{I} \sim P_G} [\log(D(\hat{I}))] - \frac{1}{2} \mathbb{E}_{\hat{I} \sim P_G} [\log(D(\hat{I}, s))] \quad (9)$$

We train the discriminators, to learn to distinguish between the real I and fake \hat{I} samples, alternately with the generators

while reducing the cross-entropy loss as below:

$$\begin{aligned} L_D = & -\frac{1}{2}\mathbb{E}_{I \sim P_{data}}[\log(D(I))] - \frac{1}{2}\mathbb{E}_{\hat{I} \sim P_G}[\log(1 - D(\hat{I}))] \\ & -\frac{1}{2}\mathbb{E}_{I \sim P_{data}}[\log(D(I, s))] - \frac{1}{2}\mathbb{E}_{\hat{I} \sim P_G}[\log(1 - D(\hat{I}, s))] \end{aligned} \quad (10)$$

where I is from the read data distribution P_{data} and \hat{I} is from the generated data distribution P_G . In Equation 10 the first and the second terms are unconditional and conditional losses as defined in [50]. Furthermore, we calculate the matching loss L_m^I between fake image vectors \hat{r} , \hat{v} and real text vectors w , s respectively, similar to the process outlined in Subsection 3.1. Hence the total loss for the TIM can be defined as:

$$L_{TIM} = L_G + \lambda_{\hat{I}} L_m^I \quad (11)$$

where $\lambda_{\hat{I}}$ is the hyper-parameter which is tuned to get better performance and the matching loss L_m^I between the generated image \hat{I}_i to real text T_i , as explained in Subsection 3.4.

3.3. ITM: Image to Text Module

The Image-to-Text branch (ITM) aims to generate fake text to assist VTA training in 3.1. It has been shown that the attention mechanism leverages the performance of image captioning models [46]. Inspired by the power and success of the transformer layer in various vision tasks [17, 15, 14, 4], we decide to use a transformer based image captioning model C as ITM.

Following the implementation of [39], we use a stack of transformer layers for the transformer encoder C_e and decoder C_d . Similar to [46], in order to pass image regional features into the transformer, we use the flattened regional feature sequence $r \in \mathbb{R}^{D \times M}$ from F_I as the input to C_e , where each column of r is a representation corresponding to a certain part of the image. As for the decoder, given the caption $T_{1:N}$ of length N , all the words prior to the target position p are embedded as $e_{1:p-1} \in \mathbb{R}^{D \times (p-1)}$, which is used as the decoder inputs to predict the p th word \hat{T}_p .

According to [4], when passing the image features into the transformer, in order to supplement the permutation-invariant issue, it's better to add positional encodings to the input of each self-attention sub-layer in C_e and encoder-decoder cross-attention sub-layer in C_d instead of only applied at the bottom of encoder. Similarly, the positional embeddings for text input are also added to the input of each self-attention sub-layer in C_d .

Taking r as input, C_e applies the same operation as Eq. (1-3) in each transformer layer and refines the regional visual features via self-attention mechanism. Then it's top output $r_e = C_e(r)$ is passed to the encoder-decoder cross-attention sub-layer within each transformer layer of C_d to further introduce the visual-language cross-attention mechanism for image-to-text generation. The sub-layer takes r_e

as keys along with the self-attention sub-layer output $\tilde{e}_{1:p-1}$ as queries:

$$\tilde{e}'_{1:p-1} = \text{Multihead}(W_Q^T \tilde{e}_{1:p-1}, W_K^T r_e, W_V^T r_e) \quad (12)$$

The decoder output is sent to MLP to predict the probability of word at position p :

$$p(\hat{T}_p | r, T_{1:p-1}) = f_s(\text{MLP}(C_d(C_e(r), e_{1:p-1}))) \quad (13)$$

Given the ground truth caption $T_{1:N}$, we train the ITM with cross-entropy loss:

$$L_{ITM} = L_C = -\sum_{p=1}^N \log(p(T_p | r, T_{1:p-1})) \quad (14)$$

3.4. Assisting losses

Given the generated images \hat{I} from TIM in Subsection 3.2 and generated texts \hat{T} from ITM in Subsection 3.3, we introduce two assisting matching losses in the model training: fake-image-real-text matching loss L_m^I and fake-text-real-image matching loss L_m^T .

Similar to L_m in Subsection 3.1, we input \hat{I} to F_I and \hat{T} to F_T to get \hat{r} , $\hat{v} = F_I(\hat{I})$ and \hat{w} , $\hat{s} = F_T(\hat{T})$. From Eq. (4-8), we can calculate the symmetric matching posterior probabilities between (\hat{I}, T) and (I, \hat{T}) , thus L_m^I and L_m^T are as:

$$\begin{aligned} L_m^I &= L_{m_s}^{T\hat{I}} + L_{m_s}^{\hat{I}T} + L_{m_w}^{T\hat{I}} + L_{m_w}^{\hat{I}T} \\ L_m^T &= L_{m_s}^{\hat{T}I} + L_{m_s}^{IT} + L_{m_w}^{\hat{T}I} + L_{m_w}^{IT} \end{aligned} \quad (15)$$

Along with L_G and L_C , our final multimodal loss for joint training is:

$$L = \lambda_m L_m + \lambda_{\hat{I}} L_m^I + \lambda_{\hat{T}} L_m^T + \lambda_G L_G + \lambda_C L_C \quad (16)$$

where $\lambda_m, \lambda_{\hat{I}}, \lambda_{\hat{T}}, \lambda_G, \lambda_C$ are hyper-parameters to add weights for each loss above.

4. Experimental Results

In this section, we explain our experiment settings, evaluation metrics and results to evaluate our proposed model.

4.1. Datasets

Our model is evaluated on two public datasets including CUB [42] and MS-COCO [25], which are widely used in text-to-image generation and image captioning tasks.

CUB is a dataset contains 200 bird species and is popular for classification, text-based image generation and image captioning tasks. It has 8855 training images and 2933 test images, where each image has 10 text descriptions. Since CUB only contains bird images with various attributes, the semantic domain is relative simple and narrow for image text representation, which is suitable for evaluating our

model in a specific semantic task. We preprocess the dataset according to the method in [47].

MS-COCO is a challenging dataset which is popular for various image-text related tasks including image captioning and image-text matching. It has 82783 training images which paired with 5 captions per image and 40504 images for testing. It provides large amounts of common object classes in the images, which can show the representation performance of our model in generalized semantic space.

4.2. Evaluation Metric

We employ R-precision a technique proposed in [47] to rank the retrieval results. To evaluate the task of reducing the heterogeneity gap between relevant word and image representation, we also propose an Attribute to Image Matching Cosine Score (AIMCoS) which matches the similarity of specific textual attributes which are supposed to be found in the paired image. Specifically, first for CUB dataset, we extract the attributes corresponding to each image file from the validation dataset. Each attribute contains text entries that list the features like color, bill length, shape, etc. of a bird. For each experiment, we first extract the global features v of the image I_i using F_I . Next, we extract the features s of textual input of each attribute associated with image. Afterwards, we compute the average of cosine similarity f_{cos} of v with the representations of each attribute corresponding to I_i . Finally, we find the mean of match scores for all the images in the validation set. Mathematically if there are K attributes present in image I_i then

$$AIMCoS = \frac{1}{U} \sum_{i=0}^{i=U} \frac{1}{K} \sum_{k=0}^{k=K} f_{cos}(v, s_k) \quad (17)$$

where U is the number of images in the validation set of CUB dataset.

For computing the AIMCoS using F_I and F_T trained on COCO dataset, each of the 80 classes are considered as attributes. We then create a smaller evaluation set (LAViT_{cocoeval}), which contains 100 images, extracted from ImageNet [7] dataset queried on the keyword. Next, similar to Eq. 17 we calculate the mean of f_{cos} between the representations of each 100 images and the representation of text the respective class name. Lastly, this score is averaged over all the classes to calculate AIMCoS for COCO dataset. In Figure 3, the larger point with label present within each cluster is the representations of the textual labels. The other points of the cluster are the representations of image data-point. The LAViT_R model is able to bridge the representational gap between textual and visual data effectively while still performing at par with other techniques.

4.3. Implementation Details

The LAViT_R model is implemented in Pytorch [29] and all the experiments are carried out on NVIDIA GTX 1080ti

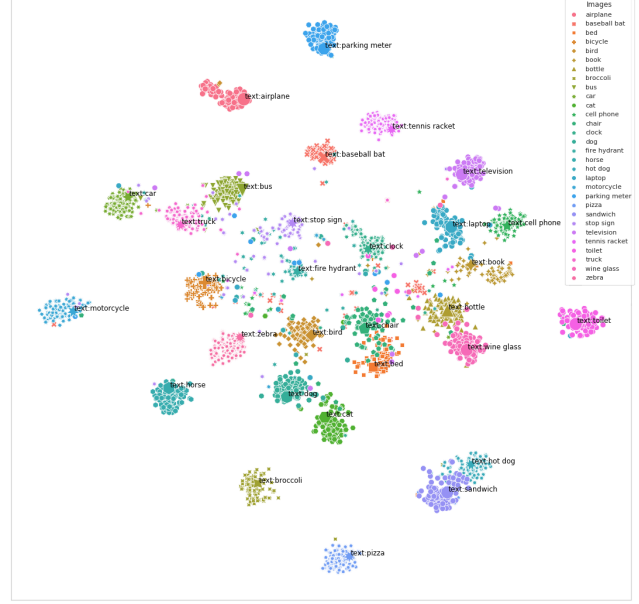


Figure 3: A T-SNE [27] visualization of 3200 image representations and 32 textual-label representations from LAViT_{cocoeval}.

GPUs. For F_I , we use the InceptionV3 model pretrained on ImageNet [7] as our backbone initialization. We use one transformer layer with 8 heads in F_T and 6 transformer layers with 8 heads in both C_e and C_d . The length of r is 289 (flattened from 17×17 feature map in F_I) and 15 for sentence length. The dimension of the word embedding and representation features r, v, w, s from VTA is 256. Three cascaded generators are used in TIM and generate fake images with resolutions 64×64 , 128×128 and 256×256 progressively.

Three training phases are designed for LAViT_R in order to make the joint training more stable and easier to converge. In phase 1, we pretrain VTA on the training data so that F_I and F_T can generate acceptable image and text representations for the following phases. We freeze F_I except the output layers for r, v , and train the transformer layer in F_T and the output layers in F_I with a learning rate 0.0002. As for phase 2, C in ITM and G in TIM are pretrained separately with the r, v, w, s features from the pretrained VTA as inputs. The learning rate is set to 0.0002 for G , and for pretraining C it is first set to 0.0001 and then decay by 0.1 after 20 epochs. When the pretrainings are completed, we freeze the first 5 layers of F_I and jointly train all the modules together as our final LAViT_R model in phase 3, with a small learning rate of 10^{-6} . All the training are optimized with the Adam optimizer [20] with a weight decay 0.0001. The batch size is set to 96 for phase 1, 32 and 14 for C and G pretraining in phase 2, and 8 for the joint training due

to the limitation of our GPU memory. In all experiments, $\gamma_1 = 4$, $\gamma_2 = 5$, $\gamma_3 = 10$ are used for the matching losses.

4.4. Performance

Hyper-parameter Selection We first adjust the λ in our multi-model loss (see Eq. 16) in order to test the effect of different loss terms in our joint training and select the best λ setting for our multi-modal loss. The results on CUB and COCO are shown in Table 1.

λ_G	λ_C	λ_{m_T}	λ_{m_I}	λ_m	R-precision	AIMCoS
0	0	0	0	1	89.76	0.5045
1	1	1	1	50	90.35	0.4931
0.01	0.1	1	1	50	90.71	0.5063
0.01	0.1	50	1	1	90.31	0.5063
0.01	0.1	1	50	1	90.49	0.496
0.01	0.1	10	1	10	90.05	0.498
0.01	0.1	10	1	1	90.19	0.501
0.001	0.1	1	0.1	10	90.16	0.501
0.01	0.1	1	1	10	90.79	0.504
1	1	1	1	1	63.4	0.203
0.01	0.1	1	5	1	62.2	0.198
0.01	0.1	5	1	1	64.6	0.197
0.01	0.1	1	1	1	63.0	0.2
0.01	0.1	1	1	10	66.4	0.202
0.01	0.1	1	1	5	66.8	0.201

Table 1: The best top-3 R-precision score of each LAViTéR model setting on COCO (top nine rows) and CUB (bottom 6 rows) test set. AIMCoS score is also reported.

As we can see, different λ settings have influenced the performance of the model. The best setting on CUB is from the bottom row in Table 1, which gives the best top-3 R-precision as 66.8%, where we choose a relative large $\lambda_m = 5$ for loss L_m while keeping small weights as $\lambda_G = 0.01$ and $\lambda_C = 0.1$ for L_G and L_C . Meanwhile, row 9 in Table 1 with a similar setting ($\lambda_m = 10$, $\lambda_G = 0.01$, $\lambda_C = 0.1$) also gives the best top-3 R-precision on COCO as 90.79%, and row 3 in Table 1 which adjusts λ_m to 50 gives the best AIMCoS score as 0.5063. These results show that L_m requires higher weight among all the loss terms, since it's a credible objective for real-image-real-text matching. On the other hand, L_m^I and L_m^T are calculated from the fake image or fake text matching, which may induce some noises in the gradients due to some low quality generated images and captions, thus smaller $\lambda_{\hat{f}}$ and $\lambda_{\hat{T}}$ gives better results. Moreover, since L_G and L_C is only used for necessary updates in G and C during joint training and has limited contribution to VTA, thus we just keep tiny weights for them.

Ablation Studies and Analysis We also conduct necessary ablation studies in Table 2 to further inspect the effect of each modules of LAViTéR. First, we set all the λ s to 0

except λ_m , which results in the worst R-precision among all the settings on COCO dataset (see the top row in Table 1). This case shows the importance of our assisting losses during the joint training. Since L_m trains the image and text encoders but has no effect on C and G , the updated feature outputs from F_I and F_T are no longer working well for the captioning model and image generator, hence the quality of generated images and captions degraded which also affects the matching performance.

In Table 2, we test the performance of LAViTéR when different modules are removed. Since symmetric global-local matching loss L_m is also used to train the image-text matching model (called DAMSM in their work) in [47, 31], so we also evaluate their performance using our metrics, which refers to AttnGAN/MirrorGAN in Table 2 and 3. DAMSM uses RNN-based text encoder in their paper instead of the transformer-based model like ours, so it also plays a role as one of our baseline. In our ablation settings, LAViTéR is our final model. $L_M(F)$ and $L_M(T)$ mean that only the VTA module is trained in phase 3 as our baseline without TIM and ITM branches, and the image encoder backbone is frozen (F , same training method as DAMSM) and trainable (T) during the joint training, respectively. LAViTéR-Img2Txt only keeps the ITM module in the joint training to generate image captions for L_m^T and the image generator G with L_m^I is removed; As a complementary setting, LAViTéR-Txt2Img keeps the image generator and L_m^I and deducts the captioning module C along with L_m^T .

As it shows in Table 2, $L_M(T)$ improves the performance for 0.66% in R-precision and 0.005 in AIMCoS, which shows that the image encoder requires update during training for a better performance. In LAViTéR-Img2Txt where G is trimmed, the R-precision drops by 0.57% from the full model and even lower than the baseline $F_M(T)$. This might be related to the large amount of unseen fake images no longer being generated and used for VTA training, thus reduces the diversity of the training set and the matching accuracy. Meanwhile, if C is removed as in LAViTéR-Txt2Img setting, both the R-precision and AIMCoS are reduced by 0.28% and 0.0023 respectively, which could be caused by lack of fake captions. When no captions are generated for matching, the training sentences and words become less various and thus affect the image-text matching performance shown in R-precision as well as the word level matching accuracy suggested by AIMCoS. On both CUB and COCO datasets, our full model LAViTéR works much better than DAMSM in [47, 31], which improves R-precision by 0.74% in COCO and 4.2% in CUB, and boosts AIMCoS from 0.44 to 0.5063 in COCO and 0.072 to 0.201 in CUB, almost 3 times better. This result shows that image-to-text and text-to-image generation branches can assist the image-text matching/representation model training

by aligning generated image with real text and generated text with real image.

We also find an interesting phenomenon in our baselines. When replacing the original RNN-based text encoder in DAMSM with our transformer-based text encoder, $L_M(F)$ has a slightly lower R-precision but much higher AIMCoS than DAMSM baseline in both Tables. This actually shows one of the main difference between transformer layer and RNN layer: due to the recurrence feature and short memory of RNN, one layer transformer may have no obvious advantage over RNN for captions with normal length around 15, which is implied in R-precision for image-caption matching; however, RNN cannot get good representations of short phrases with only 1-3 words, since it requires enough context to give reasonable outputs. In contrast, transformer’s self-attention mechanism is able to effectively handle any text length and align even a single word with the corresponding image regions, which is observed in the substantial increase in AIMCoS.

Model Name	R-precision	AIMCoS
AttnGAN/MirrorGAN[47, 31]	89.97	0.44
LAViTTeR- L_M (F)	89.81	0.501
LAViTTeR- L_M (T)	90.37	0.5059
LAViTTeR-Img2Txt	90.14	0.506
LAViTTeR-Txt2Img	90.43	0.504
LAViTTeR	90.71	0.5063

Table 2: Top-3 R-precision and Attribute Image Match Cosine Score (AIMCoS) metrics calculated on COCO dataset.

Model Name	R-precision	AIMCoS
AttnGAN/MirrorGAN [47, 31]	62.6	0.072
LAViTTeR- L_M (F)	59.2	0.184
LAViTTeR	66.8	0.201

Table 3: Top-3 R-precision and Attribute Image Match Cosine Score (AIMCoS) metrics calculated on CUB dataset.

Visualization Analysis In addition, we illustrate some qualitative results from image-to-text and text-to-image matching on COCO in Figure 4 and Figure 5 respectively. For image queries, the captions with top-5 similarity scores from our model are retrieved. Most captions are correct matches. It is observed that sentences that have “incorrect” match labels actually share similar semantics with the image queries. In Figure 5, text queries with the top-3 image matches from our model are listed. The correct matching is retrieved with other similar images, and we find that all the high ranked images are quite reasonable. These “incorrect” matching pairs with close semantics data expose a drawback in the current evaluation metrics for multi-modal

matching: many images along with their paired captions in the test set share similar semantics and are close to each other in the common semantic space, however, these neighbor samples are treated as “mismatch” in the image-to-text and text-to-image retrieval evaluation metrics and show no difference with those distinctly mismatched samples with large semantic gap. This evaluation defect motivates us to propose the new evaluation metric AIMCoS.



Figure 4: The top-5 image-to-text matching captions with descending similarity scores. Blue captions are the correct matches, while red ones are incorrect matches.



Figure 5: The top-3 text-to-image matching images with descending similarity scores from left to right. Green marks are the correct matches, while red crosses are incorrect matches.

5. Conclusion

In this paper, we introduce a novel architecture for visual and textual representation learning assisted by two auxiliary tasks, image-to-text generation and text-to-image generation. The generated images and texts are matched with real text and images to jointly train the representation model with two assisting matching losses. A new evaluation metric AIMCoS is proposed for measuring the similarity between the learnt visual and textual embedding. The experimental results on two public datasets demonstrate the effectiveness of the proposed architecture and evaluation metric.

References

- [1] C. Alberti, J. Ling, M. Collins, and D. Reitter. Fusion of detected objects in text for visual question answering. In *Proceedings of the 2019 Conference on Empirical Methods in Natural Language Processing and the 9th International Joint Conference on Natural Language Processing (EMNLP-IJCNLP)*, pages 2131–2140, 2019. 2
- [2] P. Anderson, X. He, C. Buehler, D. Teney, M. Johnson, S. Gould, and L. Zhang. Bottom-up and top-down attention for image captioning and visual question answering. In *Proceedings of the IEEE conference on computer vision and pattern recognition*, pages 6077–6086, 2018. 1, 3
- [3] Biing-Hwang Juang, Wu Hou, and Chin-Hui Lee. Minimum classification error rate methods for speech recognition. *IEEE Transactions on Speech and Audio Processing*, 5(3):257–265, 1997. 3
- [4] N. Carion, F. Massa, G. Synnaeve, N. Usunier, A. Kirillov, and S. Zagoruyko. End-to-end object detection with transformers. *arXiv preprint arXiv:2005.12872*, 2020. 5
- [5] G. Chauhan, R. Liao, W. Wells, J. Andreas, X. Wang, S. Berkowitz, S. Horng, P. Szolovits, and P. Golland. Joint modeling of chest radiographs and radiology reports for pulmonary edema assessment. In *International Conference on Medical Image Computing and Computer-Assisted Intervention*, pages 529–539. Springer, 2020. 1
- [6] Y.-C. Chen, L. Li, L. Yu, A. El Kholy, F. Ahmed, Z. Gan, Y. Cheng, and J. Liu. Uniter: Universal image-text representation learning. In *European Conference on Computer Vision*, pages 104–120. Springer, 2020. 2
- [7] J. Deng, W. Dong, R. Socher, L.-J. Li, K. Li, and L. Fei-Fei. Imagenet: A large-scale hierarchical image database. In *2009 IEEE conference on computer vision and pattern recognition*, pages 248–255. Ieee, 2009. 6
- [8] M. Denkowski and A. Lavie. Meteor universal: Language specific translation evaluation for any target language. In *Proceedings of the ninth workshop on statistical machine translation*, pages 376–380, 2014. 13
- [9] J. Devlin, M.-W. Chang, K. Lee, and K. Toutanova. BERT: Pre-training of deep bidirectional transformers for language understanding. In *Proceedings of the 2019 Conference of the North American Chapter of the Association for Computational Linguistics: Human Language Technologies, Volume 1 (Long and Short Papers)*, pages 4171–4186, Minneapolis, Minnesota, June 2019. Association for Computational Linguistics. 1
- [10] H. Fang, S. Gupta, F. Iandola, R. Srivastava, L. Deng, P. Dollár, J. Gao, X. He, M. Mitchell, J. C. Platt, C. L. Zitnick, and G. Zweig. From captions to visual concepts and back, 2015. 3
- [11] Z. Gan, Y.-C. Chen, L. Li, C. Zhu, Y. Cheng, and J. Liu. Large-scale adversarial training for vision-and-language representation learning. *arXiv preprint arXiv:2006.06195*, 2020. 2
- [12] I. J. Goodfellow, J. Pouget-Abadie, M. Mirza, B. Xu, D. Warde-Farley, S. Ozair, A. Courville, and Y. Bengio. Generative adversarial nets. In *Proceedings of the 27th International Conference on Neural Information Processing Systems - Volume 2*, NIPS’14, page 2672–2680, Cambridge, MA, USA, 2014. MIT Press. 4
- [13] K. He, X. Zhang, S. Ren, and J. Sun. Deep residual learning for image recognition. In *2016 IEEE Conference on Computer Vision and Pattern Recognition (CVPR)*, pages 770–778, 2016. 3
- [14] S. He, W. Liao, H. R. Tavakoli, M. Yang, B. Rosenhahn, and N. Pugeault. Image captioning through image transformer. *arXiv preprint arXiv:2004.14231*, 2020. 3, 5
- [15] S. Herdade, A. Kappeler, K. Boakye, and J. Soares. Image captioning: Transforming objects into words. In *Advances in Neural Information Processing Systems*, pages 11137–11147, 2019. 3, 5
- [16] M. Heusel, H. Ramsauer, T. Unterthiner, B. Nessler, and S. Hochreiter. Gans trained by a two time-scale update rule converge to a local nash equilibrium. In *Advances in neural information processing systems*, pages 6626–6637, 2017. 12
- [17] L. Huang, W. Wang, J. Chen, and X.-Y. Wei. Attention on attention for image captioning. In *Proceedings of the IEEE International Conference on Computer Vision*, pages 4634–4643, 2019. 3, 5
- [18] P.-S. Huang, X. He, J. Gao, L. Deng, A. Acero, and L. Heck. Learning deep structured semantic models for web search using clickthrough data. In *Proceedings of the 22nd ACM International Conference on Information & Knowledge Management, CIKM ’13*, page 2333–2338, New York, NY, USA, 2013. Association for Computing Machinery. 3
- [19] Y. Huang, W. Wang, and L. Wang. Instance-aware image and sentence matching with selective multimodal lstm. In *Proceedings of the IEEE Conference on Computer Vision and Pattern Recognition*, pages 2310–2318, 2017. 2
- [20] D. P. Kingma and J. Ba. Adam: A method for stochastic optimization. *arXiv preprint arXiv:1412.6980*, 2014. 6
- [21] G. Li, N. Duan, Y. Fang, M. Gong, and D. Jiang. Unicodervl: A universal encoder for vision and language by cross-modal pre-training. In *The Thirty-Fourth AAAI Conference on Artificial Intelligence, AAAI 2020, The Thirty-Second Innovative Applications of Artificial Intelligence Conference, IAAI 2020, The Tenth AAAI Symposium on Educational Advances in Artificial Intelligence, EAAI 2020, New York, NY, USA, February 7-12, 2020*, pages 11336–11344. AAAI Press, 2020. 2

- [22] L. H. Li, M. Yatskar, D. Yin, C.-J. Hsieh, and K.-W. Chang. Visualbert: A simple and performant baseline for vision and language, 2019. 2
- [23] X. Li, X. Yin, C. Li, P. Zhang, X. Hu, L. Zhang, L. Wang, H. Hu, L. Dong, F. Wei, et al. Oscar: Object-semantics aligned pre-training for vision-language tasks. In *European Conference on Computer Vision*, pages 121–137. Springer, 2020. 2
- [24] Y. Li, H. Wang, and Y. Luo. A comparison of pre-trained vision-and-language models for multimodal representation learning across medical images and reports. *arXiv preprint arXiv:2009.01523*, 2020. 1
- [25] T.-Y. Lin, M. Maire, S. Belongie, J. Hays, P. Perona, D. Ramanan, P. Dollár, and C. L. Zitnick. Microsoft coco: Common objects in context. In *European conference on computer vision*, pages 740–755. Springer, 2014. 5, 11, 12
- [26] J. Lu, D. Batra, D. Parikh, and S. Lee. Vilbert: Pretraining task-agnostic visiolinguistic representations for vision-and-language tasks. In *Advances in Neural Information Processing Systems*, pages 13–23, 2019. 2
- [27] L. v. d. Maaten and G. Hinton. Visualizing data using t-sne. *Journal of machine learning research*, 9(Nov):2579–2605, 2008. 6
- [28] M. Mirza and S. Osindero. Conditional generative adversarial nets, 2014. 4
- [29] A. Paszke, S. Gross, F. Massa, A. Lerer, J. Bradbury, G. Chanan, T. Killeen, Z. Lin, N. Gimelshein, L. Antiga, A. Desmaison, A. Kopf, E. Yang, Z. DeVito, M. Raison, A. Tejani, S. Chilamkurthy, B. Steiner, L. Fang, J. Bai, and S. Chintala. Pytorch: An imperative style, high-performance deep learning library. In H. Wallach, H. Larochelle, A. Beygelzimer, F. d’Alché-Buc, E. Fox, and R. Garnett, editors, *Advances in Neural Information Processing Systems 32*, pages 8024–8035. Curran Associates, Inc., 2019. 6
- [30] G. Peyré, M. Cuturi, et al. Computational optimal transport: With applications to data science. *Foundations and Trends® in Machine Learning*, 11(5–6):355–607, 2019. 2
- [31] T. Qiao, J. Zhang, D. Xu, and D. Tao. Mirrorgan: Learning text-to-image generation by redescription. In *Proceedings of the IEEE Conference on Computer Vision and Pattern Recognition*, pages 1505–1514, 2019. 2, 7, 8, 11, 12
- [32] S. Reed, Z. Akata, X. Yan, L. Logeswaran, B. Schiele, and H. Lee. Generative adversarial text to image synthesis. In *33rd International Conference on Machine Learning*, pages 1060–1069, 2016. 2
- [33] S. Ren, K. He, R. Girshick, and J. Sun. Faster r-cnn: Towards real-time object detection with region proposal networks. In *Advances in neural information processing systems*, pages 91–99, 2015. 2, 3
- [34] T. Salimans, I. Goodfellow, W. Zaremba, V. Cheung, A. Radford, and X. Chen. Improved techniques for training gans. arxiv 2016. *arXiv preprint arXiv:1606.03498*. 12
- [35] W. Su, X. Zhu, Y. Cao, B. Li, L. Lu, F. Wei, and J. Dai. Vi-bert: Pre-training of generic visual-linguistic representations. In *International Conference on Learning Representations*, 2019. 2
- [36] C. Szegedy, V. Vanhoucke, S. Ioffe, J. Shlens, and Z. Wojna. Rethinking the inception architecture for computer vision. In *2016 IEEE Conference on Computer Vision and Pattern Recognition (CVPR)*, pages 2818–2826, 2016. 3
- [37] H. Tan and M. Bansal. LXMERT: Learning cross-modality encoder representations from transformers. In *Proceedings of the 2019 Conference on Empirical Methods in Natural Language Processing and the 9th International Joint Conference on Natural Language Processing (EMNLP-IJCNLP)*, pages 5100–5111, Hong Kong, China, Nov. 2019. Association for Computational Linguistics. 2
- [38] S. Uppal. CA:TR: Image captioning with transformers. <https://github.com/saahiluppal/catr>. 14
- [39] A. Vaswani, N. Shazeer, N. Parmar, J. Uszkoreit, L. Jones, A. N. Gomez, Ł. Kaiser, and I. Polosukhin. Attention is all you need. In *Advances in neural information processing systems*, pages 5998–6008, 2017. 3, 4, 5
- [40] R. Vedantam, C. Lawrence Zitnick, and D. Parikh. Cider: Consensus-based image description evaluation. In *Proceedings of the IEEE conference on computer vision and pattern recognition*, pages 4566–4575, 2015. 13
- [41] O. Vinyals, A. Toshev, S. Bengio, and D. Erhan. Show and tell: A neural image caption generator. In *Proceedings of the IEEE conference on computer vision and pattern recognition*, pages 3156–3164, 2015. 3, 13, 14
- [42] C. Wah, S. Branson, P. Welinder, P. Perona, and S. Belongie. The caltech-ucsd birds-200-2011 dataset. 2011. 5, 12
- [43] L. Wang, Y. Li, J. Huang, and S. Lazebnik. Learning two-branch neural networks for image-text matching tasks. *IEEE Transactions on Pattern Analysis and Machine Intelligence*, 41(2):394–407, 2018. 2
- [44] X. Wei, T. Zhang, Y. Li, Y. Zhang, and F. Wu. Multi-modality cross attention network for image and sentence matching. In *Proceedings of the IEEE/CVF Conference on Computer Vision and Pattern Recognition*, pages 10941–10950, 2020. 2
- [45] Xiaodong He, Li Deng, and Wu Chou. Discriminative learning in sequential pattern recognition. *IEEE Signal Processing Magazine*, 25(5):14–36, 2008. 3
- [46] K. Xu, J. Ba, R. Kiros, K. Cho, A. Courville, R. Salakhudinov, R. Zemel, and Y. Bengio. Show, attend and tell: Neural image caption generation with visual attention. In *International conference on machine learning*, pages 2048–2057, 2015. 3, 5, 13, 14
- [47] T. Xu, P. Zhang, Q. Huang, H. Zhang, Z. Gan, X. Huang, and X. He. Attngan: Fine-grained text to image generation with attentional generative adversarial networks. In *Proceedings of the IEEE conference on computer vision and pattern recognition*, pages 1316–1324, 2018. 2, 3, 4, 6, 7, 8, 11, 12, 14
- [48] Z. Yang, Z. Dai, Y. Yang, J. Carbonell, R. R. Salakhutdinov, and Q. V. Le. Xlnet: Generalized autoregressive pretraining for language understanding. In *Advances in neural information processing systems*, pages 5753–5763, 2019. 1
- [49] T. Yao, Y. Pan, Y. Li, and T. Mei. Exploring visual relationship for image captioning. In *Proceedings of the European conference on computer vision (ECCV)*, pages 684–699, 2018. 3

- [50] H. Zhang, T. Xu, H. Li, S. Zhang, X. Wang, X. Huang, and D. N. Metaxas. Stackgan++: Realistic image synthesis with stacked generative adversarial networks. *IEEE Transactions on Pattern Analysis and Machine Intelligence*, 41(8):1947–1962, 2019. [2](#), [5](#), [12](#)
- [51] L. Zhou, H. Palangi, L. Zhang, H. Hu, J. J. Corso, and J. Gao. Unified vision-language pre-training for image captioning and VQA. In *The Thirty-Fourth AAAI Conference on Artificial Intelligence, AAAI 2020, The Thirty-Second Innovative Applications of Artificial Intelligence Conference, IAAI 2020, The Tenth AAAI Symposium on Educational Advances in Artificial Intelligence, EAAI 2020, New York, NY, USA, February 7-12, 2020*, pages 13041–13049. AAAI Press, 2020. [3](#)
- [52] J.-Y. Zhu, T. Park, P. Isola, and A. A. Efros. Unpaired image-to-image translation using cycle-consistent adversarial networks. In *Proceedings of the IEEE international conference on computer vision*, pages 2223–2232, 2017. [2](#)

Appendices

Below we mention some analysis and downstream tasks performed using our pre-trained encoders.

A. VTA Qualitative Results

Apart from the T-SNE visualization in main paper, we also plot the Image representation vs Token representation similarity map in Figure 6.

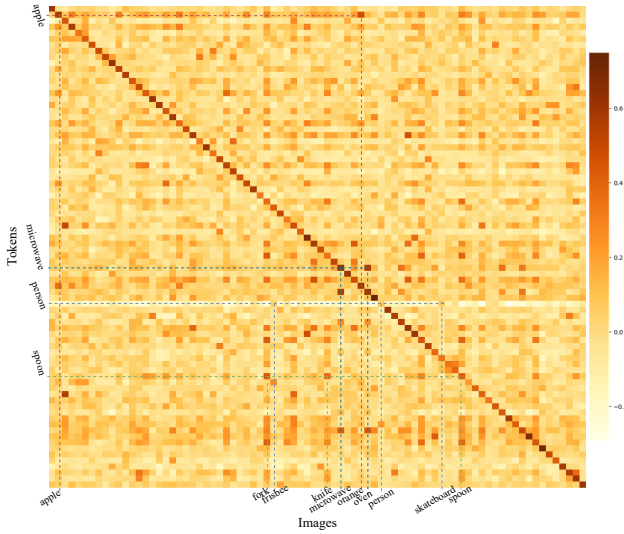


Figure 6: Visualization of Image representation vs Token representation similarity map

The x-axis denotes the image representations and the y-axis denotes the category word token representation. Since

there are 80 classes in COCO dataset [25], the matrix size is 80×80 . There are 80 Tokens and 8000 images, i.e. 100 images per token. We first compute similarity of each token representation with all the 8000 images in LaViTeR_{cocoeval} dataset. Then, the average similarity value of match with each token plotted in Figure 6. The dark color diagonal shows a high similarity between true matches, indicating the efficacy of LAViTTeR model.

From Figure 6, we observe that, the token “apple” matches highest with the images of apple but also contains high similarity with images of another fruits like “orange” because they are usually kept together. Similarly, the token “microwave” is highly matched with images of “microwave” and also with “oven” and in reality most of the times they appear together. More interestingly, the token “person” is not matched with other images showing no correlation, but is matched highly with images of “person” and also “skateboard” as in many “skateboard” images there is a person in the frame. Also, the token “spoon” is highest matched with “spoon” images and also slightly matched with images of “fork” and “knife” as these items usually appear together naturally. Thus, the joint training is able to reduce the diversity gap between the nature of textual and visual representations meaningfully.

B. TIM Qualitative Results

Although our primary goal is not to improve GAN, we compare the quality of generated images from LAViTTeR model with the ground truth and the generated images by [31, 47]. Those examples are selected from the visualization of the previous state-of-the-art papers directly.

As can be seen from Figure 7 and 8, the LAViTTeR model is able to perform at-par and in some cases better than the previous state-of-the-art models. We do not report these images in the main paper as the major goal of LAViTTeR is for representation joint learning and alignment. The model is able to perform better due to continuous training of VTA, TIM and ITM models cooperatively. The generated images during the training process are able to provide a diverse set of images, which further assists the joint learning and also the GAN module.

Model	IS \uparrow	FID \downarrow
StackGAN-v1	8.45 ± 0.03	74.05
StackGAN-v2	8.30 ± 0.10	81.59
AttnGAN	25.89 ± 0.47	-
MirrorGAN	26.47 ± 0.41	-
LAViTTeR	26.71 ± 0.39	75.5

Table 4: IS and FID scores, calculated on COCO 2014 validation set. Up arrow means higher value is better, down arrow means lower value better.

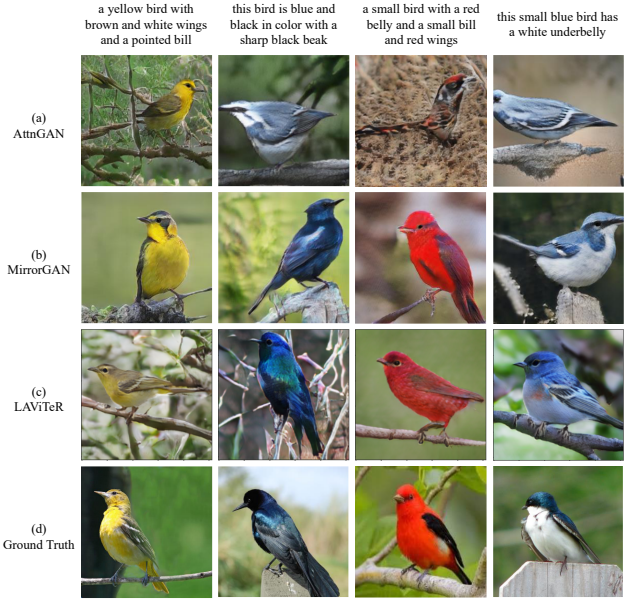


Figure 7: Examples of images generated by (a) AttnGAN [47], (b) MirrorGAN [31] (c) LaViTeR network (d) the corresponding ground truth. Left four columns are images from CUB [42] dataset.

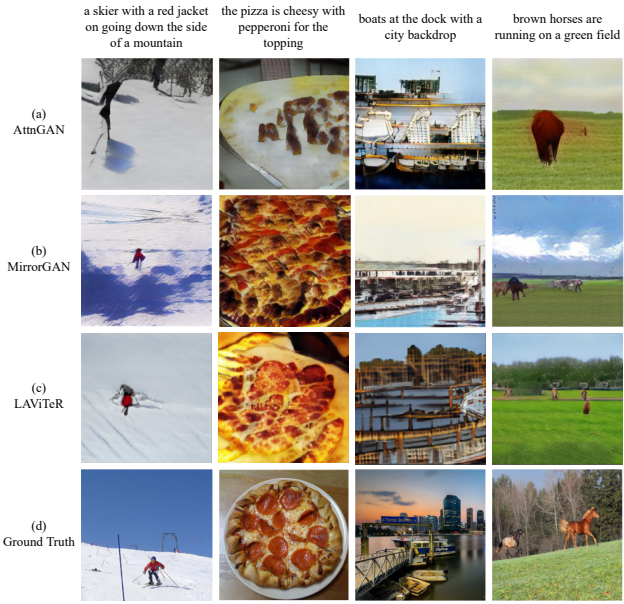


Figure 8: Examples of images generated by (a) AttnGAN [47], (b) MirrorGAN [31] (c) LaViTeR network (d) the corresponding ground truth. Left four columns are images from COCO [25] dataset.

We also compute the Inception Score (IS) [34] and Fréchet Inception Distance (FID) [16] to compare the GAN module trained while joint learning. Table 4 shows that GAN in LaViTeR model performs better than all the previous models in terms of IS Score while the FID score is still comparable to other text to image network as [50] that report FID scores. However, better GAN performance is a by-product of LAViTTeR model, not it's goal.

C. ITM Qualitative Results

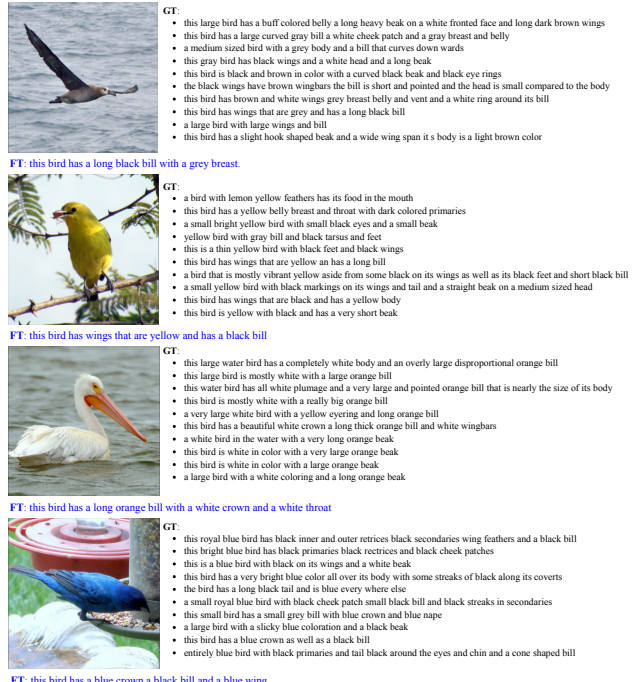


Figure 9: Examples of generated captions (FT (Fake Text) in blue under sample images) by LAViTTeR ITM and the corresponding ground truth captions (GT in black).

Some examples of generated captions by our LAViTTeR ITM branch are shown in Figure 9 and Figure 10. As Figure 9 shows, the generated captions are able to capture the main attributes (crown color, bill size, breast color, etc.) of the birds in sample images from CUB test set. Figure 10 shows objects and their corresponding actions and attributes in sample images from COCO test set. Specifically, some of the generated captions can generate words (marked in red) that are not included in the ground truth captions, but actually shown up in the images. Some objects in the background are predicted in the generated captions, e.g. for the first image in the third row, ‘trees’ is in the background of the image which is never described in the paired ground truth captions, but successfully predicted by



- two young boys are enjoying pizza and pepsi
- Two young boys sit at a table with pizza.
- A couple of kids at a table with some food.
- Two small children sit at the table and eat pizza
- Two little boys eating pizza and soda at school.

FT: Two children sitting at a table with a plate of food.



- A horse drawn buggy sits in front of pyramid shaped mosques.
- A horse hitched to a cart standing in front of a temple.
- The horse stands attached to an empty carriage.
- There is a horse pulling a carriage.
- A horse carriage is sitting idly in the dessert.

FT: A horse drawn carriage on a dirt road.



- A man standing in a living room holding a Nintendo Wii game controller.
- Three people with cups on the couch and one with remote standing
- A man holding a motion controlled video game controller
- Man with video game controller in living room with onlooker seated nearby.
- A man playing a video game while two men sit on a couch.

FT: A group of people sitting on a couch playing a video game.



- A white toilet sitting in a bathroom stall next to a TP dispenser.
- A white toilet sits in a bathroom, with the lid open.
- A small, white toilet with a toilet paper dispenser on the wall.
- A toilet is placed within a shower stall.
- A toilet right next to a shower stall.

FT: A toilet with the lid up in a bathroom.



- The reflection of a dogs head out of a car window in one of the cars wing mirrors
- An adorable brown and white dog hanging it's head out of a window.
- a dog has its head hanging out of a window
- A dog looking out the window as seen through a mirror.
- A dog that is sitting down in a backseat.

FT: A dog sticking its head out of a car window.



- A man flying through the air while riding a bike.
- A person jumping in the air on a motorcycle
- MOTOR CROSS BIKE AND RIDER IN THE AIR DOING TRICKS
- a man in mid air while riding a motor bike
- A person who is on their motorcycle in the air.

FT: A person on a motorcycle flying through the air.



- A couple of people riding a pair of skis down a snow covered slope.
- a couple of people skiing down a snowy slope
- THERE ARE PEOPLE THAT ARE ON THE SNOW SLOPE SKIING
- two snow skiers are coming down a hill
- The cross country skiers are enjoying their run.

FT: A person on skis in the snow with trees in the background.



- A stop sign at the end of the road.
- A snow covered road with a stop sign next to it.
- A stop sign on a corner of a snowy road.
- A stop sign is standing next to a road in the snow.
- An icy snow covered road overlooking a body of water.

FT: A stop sign on a snowy road near a body of water



- a man wearing a top hat and a red tie
- A very sharp dressed man with a black top hat.
- A man with black hair and a top hat
- A man with a top hat and a red tie.
- A man wearing a top hate with a red tie and black shirt.

FT: A man in a hat and a tie is smiling.



- A black and white picture of a large house is shown.
- A tree stands next to an old wood house
- an older home with multiple windows, shot from the street.
- A three-story Victorian-era frame house with a peaked roof.
- a house is sitting on an empty block

FT: A street sign on a pole on a city street



- Side of meat sitting on a white plate on a dinner table.
- A plate of food at the table with meat
- Some interesting food sitting on a white plate by a knife
- Here is a plate of food that appears to have been browned in butter.
- A white plate topped with food sitting on a table.

FT: A plate of food with a fork and knife on it.



- A hotel suite with balcony overlooking the scenery
- A large living area with a bed and some couches
- There is a living room with a wide open view
- A living room with white furniture and a small wooden table.
- A bedroom suite with balcony and lovely view

FT: A living room with a couch, coffee table, and a television.

Figure 10: Examples of generated captions (FT (Fake Text) in blue under sample images) by LaViTeR ITM and the corresponding ground truth captions (in black). The objects or attributes shown in the sample image but not in its ground truth descriptions are marked in red.

Model	BLEU-1	BLEU-2	BLEU-3	BLEU-4	METEOR	CIDEr
Show-tell [41]	-	-	-	27.7	23.7	85.5
Show-attend-tell [46]	70.7	49.2	34.4	24.3	23.9	-
LAViTéR	69.15	51.75	37.68	27.44	24.20	86.72

Table 5: BLEU 1-4, METEOR[8] and CIDEr[40] scores of our ITM module calculated on MSCOCO 2014 validation set. Results reported in [41] and [46] are also listed here for reference.

ITM; for the last image, TV and coffee table are shown in the background corner of the image and are ignored by the ground truth texts, but are captured by the generated caption. Even only a part of the object appears in an image, it still has a chance to show up in our generated caption, e.g. in the image in the middle of the last row, a tiny part of a

fork tip appears on the left, our ITM can generate ‘a fork’ given such a small clue in the image. Missing attributes are also predicted such as the attribute ‘smiling’ is generated in our generated text, which is never described in the ground truths. These generated texts from ITM with the missing objects and attributes in the original images pro-

vide further useful information outside the training dataset and help the matching model learn more word-region level matching pairs. This is exactly one of our motivations for our LAViTéR method.

We also evaluate the captioning ability of our ITM branch from the joint training, listed in Table 5. As we can see, our ITM can get a comparable result with other captioning models, such as [46] and [41], which shows that our ITM has the ability to generate reasonable captions for real-image-fake-text matching training. Note that we are not aiming at coming up with a novel and state-of-the-art captioning model, the main function of ITM branch is to provide more reasonable fake text for training the VTA matching model.

D. Code

Our code referenced from libraries open sourced by the work done in CATR [38] and AttnGAN [47].